AIAA JOURNAL
Vol. 40, No. 7, July 2002

More Photogrammetry for Wind-Tunnel Testing

Wim Ruyten*
Jacobs Sverdrup, Arnold Air Force Base, Tennessee 37389-4300

Recent work by Liu et al. (Liu, T., Cattafesta, L. N., III, Radeztsky, R. H., and Burner, A. W., "Photogrammetry Applied to Wind-Tunnel Testing," *AIAA Journal*, Vol. 38, No. 6, 2000, pp. 964–971) has led to renewed interest in the use of photogrammetry for measuring the position, attitude, and deformation of a test article in a wind tunnel. The present research expands on this work with a more comprehensive mathematical model that can be used not only for determining the interior parameters of the cameras, but also the wind-off alignment of both the cameras and the test article relative to the wind tunnel. This calibration is achieved by combining data from multiple cameras and multiple model attitude settings in a single least-squares fit, though (with eight cameras) as many as 94 fit parameters can be involved. Similarly, data from multiple cameras are combined in a single six-parameter fit to determine the position and attitude of the test article at wind-on conditions. Precision estimates of fitted parameters are obtained through use of the covariance-matrix formalism and by bootstrapping. The model is demonstrated on data from two pressure-sensitive paint tests. An absolute accuracy of 0.01 deg for pitch measurements is demonstrated for this nonoptimized configuration. Suggestions for improvements are given for a dedicated optical model attitude measurement system.

I. Introduction

In a recent paper[1] Liu et al. describe the use of photogrammetry to wind-tunnel testing. In essence, this is the application of photographic methods (now mostly digital) to the measurement of position, attitude, and deformation of an object, in this case, a test article in a wind tunnel. Interest in photogrammetry is increasing for several reasons: 1) The technique is nonintrusive and does not require wiring of the model; 2) accuracy can approach that of gravity-sensing inclinometers for measurement of pitch and roll,[2–4] while being more sensitive to yaw; 3) photogrammetry lends itself to companion optical techniques such as luminescent paint measurements[5–9]; 4) bias error corrections caused by dynamics are not required, as is the case for inclinometers.[10]

Broadly speaking, application of photogrammetric methods can be divided into two tasks: calibration of the instrument (that is, the cameras) and use of the instrument to measure displacements, orientations, deflections, and so on.[11–13] The paper by Liu et al. focuses on the first task, particularly the calibration of the interior parameters of the cameras. These are the principal point and principal distance and a set of parameters that describe deviations from a purely linear imaging process. In addition, for each camera a set of six exterior parameters needs to be specified to describe the position and orientation of the camera relative to a reference coordinate system. Liu et al. propose a single-point calibration in which a camera is mounted in the wind tunnel, and a calibration object (for example, a multistep block with known target locations) is placed in the field of view. This leaves the task of relating the coordinates of the calibration object to those of the wind tunnel. A similar single-point calibration is described by Ruyten based on use of the test article itself,[2] on which are placed a number of registration targets. A drawback of both single-point approaches is that they may require corrections for misalignments between the model and the wind tunnel. For example, it is shown in Ref. 2 that because of a roll misalignment an apparent yawing component is introduced during a pure pitch sweep of the test article. To account for such misalignments, a multipoint calibration is introduced here. In it (Fig. 1) the positions and orientations of multiple cameras relative to the wind tunnel are derived from images of the test article at a range of attitude settings of the model support system. Included in this calibration is a precise determination of the alignment of the test article relative to the tunnel. To implement the multipoint, multicamera calibration, the conventional photogrammetry model is expanded to include explicitly the alignment and motion of the test article relative to the wind tunnel. A new approach is advocated in which data from multiple cameras are combined in a single least-squares fit, both for calibration purposes and for optical model position and attitude determination. This approach allows for a more comprehensive treatment of measurement precision than is achieved in Refs. 1 and 2. The ensuing mathematical model also can be used as the basis for automatic image registration, as is reported in Ref. 14. An earlier version of the present work has appeared as Ref. 15.

II. Theory

The analytical challenges of photogrammetry for wind-tunnel testing considered here are calibration of the instrument (that is, determination of the interior and exterior parameters of the cameras) and use of the cameras to measure position and attitude of a test article. Three coordinate systems play a role in the analysis.

The first is the model coordinate system, which is typically defined by the test customer. Model coordinates of registration targets on the test article are defined in this coordinate system, for example, through the use of a coordinate measuring machine. Model coordinates are independent of the placement and orientation of the test article. Changes in model coordinates caused by deformation of the test article are not considered here.

The second set of coordinates (to be denoted with an asterisk) is that associated with the test facility. This is the tunnel coordinate system with respect to which are to be determined the fixed locations and orientations of the cameras and the variable position and attitude of the test article.

The third type of coordinate system is that associated with individual cameras. Image coordinates of the registration targets are expressed in image pixels, typically with fractional values due to subpixel centering.

A. Imaging Process

As is common in photogrammetry, the imaging process is described by the projective transform. Let i denote a point on the test article with model coordinates (x_i, y_i, z_i) and tunnel coordinates $(x^*_{ki}, y^*_{ki}, z^*_{ki})$, where k denotes a specific attitude setting of the model support system. When viewed by an ideal camera c (that is, without lens distortion), the image coordinates (in pixels) of point i would be given by

Received 26 June 2001; revision received 2 January 2002; accepted for publication 17 January 2002.

*Engineer Specialist, AEDC Group, Instrumentation and Diagnostics Branch, 609 Second Street. Senior Member AIAA.

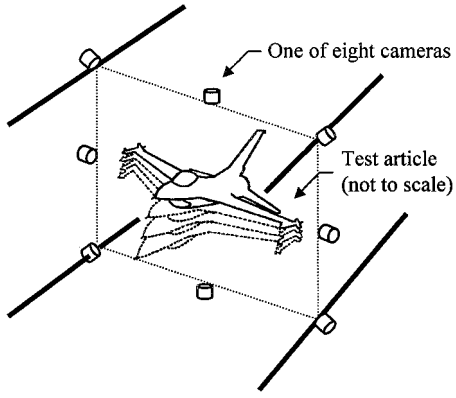

Fig. 1 Application of multipoint, multicamera photogrammetry technique in AEDC 16-ft transonic wind tunnel.

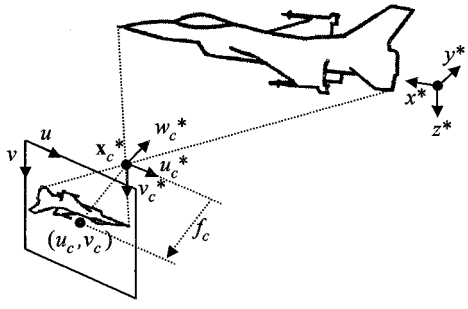

Fig. 2 Illustration of imaging process with respect to tunnel coordinate system.

$$u_{kci}^{(0)} = u_c - f_c(U_{kci}/W_{kci}), \qquad v_{kci}^{(0)} = v_c - f_c a_c(V_{kci}/W_{kci}) \quad (1)$$

where (working in tunnel coordinates):

$$U_{kci} = u_{xc}^*\left(x_{ki}^* - x_c^*\right) + u_{yc}^*\left(y_{ki}^* - y_c^*\right) + u_{zc}^*\left(z_{ki}^* - z_c^*\right)$$

$$V_{kci} = v_{xc}^*\left(x_{ki}^* - x_c^*\right) + v_{yc}^*\left(y_{ki}^* - y_c^*\right) + v_{zc}^*\left(z_{ki}^* - z_c^*\right)$$

$$W_{kci} = w_{xc}^*\left(x_{ki}^* - x_c^*\right) + w_{yc}^*\left(y_{ki}^* - y_c^*\right) + w_{zc}^*\left(z_{ki}^* - z_c^*\right) \quad (2)$$

In Eq. (1), (u_c, v_c) and f_c are the principal point and principal distance of camera c in image pixels, and a_c is the ratio of row and column spacings on the sensor array. In Eq. (2), x_c^*, y_c^*, and z_c^* specify the position of camera c with respect to the wind tunnel. The nine components $u_{xc}^* \ldots w_{zc}^*$ are elements of an othonormal orientation matrix $\boldsymbol{m}_c^*$ that can be expressed in terms of a set of camera Euler angles ϕ_c^*, κ_c^*, and ω_c^* as follows:

$$\boldsymbol{m}_c^* = \begin{pmatrix} u_{xc}^* & u_{yc}^* & u_{zc}^* \\ v_{xc}^* & v_{yc}^* & v_{zc}^* \\ w_{xc}^* & w_{yc}^* & w_{zc}^* \end{pmatrix} = \boldsymbol{R}\left(\phi_c^*, \kappa_c^*, \omega_c^*\right) \quad (3)$$

Different definitions of the Euler matrix $\boldsymbol{R}$ are possible. Here, the definition of Eq. (A1) from Appendix A is used. The rows of the matrix $\boldsymbol{m}_c^*$ can be thought of as an orthonormal set of unit vectors $\boldsymbol{u}_c^*$, $\boldsymbol{v}_c^*$, and $\boldsymbol{w}_c^*$ in tunnel space that define the axes of the camera array and the viewing direction of camera c, respectively (Fig. 2).

In practice, lens distortion causes a deviation from the ideal imaging process implied by Eq. (1). The resulting image coordinates u_{kci} and v_{kci} can be expressed in terms of the undistorted coordinates from Eq. (1) by[1,12,13]

$$u_{kci} = u_{kci}^{(0)} - \delta_{ukci}, \qquad v_{kci} = v_{kci}^{(0)} - \delta_{vkci} \quad (4)$$

The distortion terms can be expressed in terms of a radial distortion parameter K_{1c} by

$$\delta_{ukci} = K_{1c}\left[u_{kci}^{(0)} - u_c\right]\left\{\left[u_{kci}^{(0)} - u_c\right]^2 + \left[v_{kci}^{(0)} - v_c\right]^2\right\}$$

$$\delta_{vkci} = K_{1c}\left[v_{kci}^{(0)} - v_c\right]\left\{\left[u_{kci}^{(0)} - u_c\right]^2 + \left[v_{kci}^{(0)} - v_c\right]^2\right\} \quad (5)$$

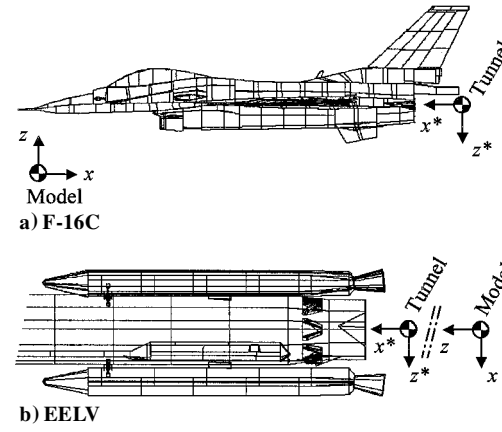

Fig. 3 Nominal relation of model coordinate system and AEDC tunnel coordinate system for two types of test article.

Higher-order distortion terms can be added, for example, when working with short focal length lenses.

B. Model Alignment

To proceed, the tunnel coordinates $(x_{ki}^*, y_{ki}^*, z_{ki}^*)$ of the point i must be related to its model coordinates (x_i, y_i, z_i). This is done in two steps, by specifying an initial alignment at some reference setting of the model support system and subsequent motion away from this reference setting. The reference setting is conceived as a virtual set point. It is thus not necessary that the model support system ever be positioned exactly at this setting (which may be impossible as a result of slack in the tunnel hardware). To emphasize the virtual nature of the reference setting, it is denoted with the index $k = 0$. Actual set points are labeled with $k = 1, 2, 3$, etc. At the reference setting the relationship between the model coordinates (x_i, y_i, z_i) and tunnel coordinates $(x_{0i}^*, y_{0i}^*, z_{0i}^*)$ is assumed to be given by

$$\boldsymbol{x}_{0i}^* = \Delta\boldsymbol{x}_m + \boldsymbol{R}_m\boldsymbol{x}_i \quad (6)$$

Here $\Delta\boldsymbol{x}_m$ denotes a displacement vector with components $(\Delta x_m, \Delta y_m, \Delta z_m)$, and $\boldsymbol{R}_m$ denotes an alignment matrix that is given in terms of three Euler angles α_m, β_m, and ϕ_m by Eq. (A1) according to

$$\boldsymbol{R}_m = \boldsymbol{R}(\alpha_m, \beta_m, \phi_m) \quad (7)$$

Figure 3 shows two examples for the Arnold Engineering Development Center (AEDC) 16-ft transonic wind tunnel, which employs a tunnel coordinate system with an x^* axis pointing upstream and a z^* axis pointing down. In this case (Fig. 3a) the model coordinate axes in x and z are typically opposite to those of the tunnel, with nominal alignment angles $\alpha_m = 0$ deg, $\beta_m = 180$ deg, and $\phi_m = 180$ deg. Alternatively (Fig. 3b), the model x, y, and z axes can be cyclically permutated from the tunnel axes, giving rise to nominal alignment angles $\alpha_m = 0$ deg, $\beta_m = 90$ deg, and $\phi_m = -90$ deg. In both cases a large axial displacement Δx_m must typically be specified. A smaller vertical displacement Δz_m must typically be specified as well in Fig. 3a. In practice, all six alignment parameters (that is, the parameters Δx_m, Δy_m, Δz_m, α_m, β_m, and ϕ_m) may be known only approximately at the start of the test. An important part of the multipoint calibration in Sec. II.D is to determine these parameters with greater precision.

C. Model Motion

To complete the theoretical framework, the motion of the test article away from the virtual reference setting from Sec. II.B must be specified. Rigid-body motion is assumed. The tunnel coordinates of a point i at an attitude setting k (with $k = 1, 2, 3, \ldots$) can then be expressed as

$$\boldsymbol{x}_{ki}^* = \Delta\boldsymbol{x}_k + \boldsymbol{R}_k\boldsymbol{x}_{0i}^* \quad (8)$$

Here $\Delta\boldsymbol{x}_k$ denotes a displacement vector with components $(\Delta x_k, \Delta y_k, \Delta z_k)$, and $\boldsymbol{R}_k$ denotes a model attitude matrix that is given in terms of three Euler angles α_k, β_k, and ϕ_k by Eq. (A1) according to

$$\boldsymbol{R}_k = \boldsymbol{R}(\alpha_k, \beta_k, \phi_k) \quad (9)$$

When using photogrammetry to determine model attitudes, the angles α_k, β_k, and ϕ_k are the object of the measurement. During calibration, the displacement vector $\Delta \boldsymbol{x}_k$ and attitude matrix $\boldsymbol{R}_k$ are taken to be those of the model support system and are denoted with an additional subscript zero. That is, when Eqs. (8) and (9) are used for calibration, they are written as

$$\boldsymbol{x}^*_{ki} = \Delta \boldsymbol{x}_{0k} + \boldsymbol{R}_{0k} \boldsymbol{x}^*_{0i} \tag{8'}$$

with

$$\boldsymbol{R}_{0k} = \boldsymbol{R}(\alpha_{0k}, \beta_{0k}, \phi_{0k}) \tag{9'}$$

By proper selection of the origin of the tunnel coordinate system, it is possible to set all or most of the components of the displacement vector $\Delta \boldsymbol{x}_{0k}$ to zero. For example, for the AEDC 16-ft tunnel $\Delta \boldsymbol{x}_{0k} = (0, 0, 0)$ when the origin of the tunnel coordinate system is chosen at the pitch-roll center of the model support system, as is done in Fig. 3. Moreover, for the AEDC case, if the virtual reference setting is selected to be that for which pitch, yaw, and roll of the model support system are zero, the angles in Eq. (9′) are given by $\alpha_{0k} =$ ALPI, $\beta_{0k} = 0$ deg, and $\phi_{0k} =$ PHII, where ALPI and PHII are the readout values from the model support system.

D. Photogrammetry Tasks

When combined, Eqs. (1–9) express the image coordinates (u_{kci}, v_{kci}) of a target point i for camera c at a model attitude setting k as a function of these groups of parameters: 1) the target coordinates (x_i, y_i, z_i) in model space; 2) the camera interior parameters u_c, v_c, f_c, a_c, and K_{1c}; 3) the camera exterior parameters x^*_c, y^*_c, z^*_c, ϕ^*_c, κ^*_c, and ω^*_c; 4) the model alignment parameters Δx_m, Δy_m, Δz_m, α_m, β_m, and ϕ_m; and 5) the model position and attitude parameters Δx_k, Δy_k, Δz_k, α_k, β_k, and ϕ_k (possibly with an additional subscript zero to indicate calibration settings).

Application of photogrammetry in the present context can now be defined as measurement of a subset of these values, given values for the other parameters. Table 1 lists the tasks that are considered in this work. Bold print is used to indicate which parameters are to be determined, either by explicit calculation or by iterative least-squares optimization (see Sec. II.E). Entries "K" in Table 1 denote values that are known either through measurement, estimation, or readout from the model support system ("sting" in Table 1).

The tasks in Table 1 are listed in the order in which they are typically performed. In step 1 a single-point calibration is performed for each camera separately, using a single attitude setting of the model support system. At this point the user supplies estimated values of the model alignment parameters. Initial values of the camera parameters either can be estimated or obtained in step 1a by an explicit calculation that is based on a direct linear transform of measured image coordinates (see Appendix B).[16] In step 1 it may be necessary to hand select registration targets in one image for each camera. During processing of subsequent images, it should be possible to identify registration targets automatically, using the predictions from step 2 in Table 1 and the techniques from Ref. 14. A possible exception is the case in which initial estimates of the model alignment parameters are poor. In this case it may not be possible to predict accurately the image coordinates of registration targets at attitude settings significantly away from the setting at which the single-point calibration was performed. The remedy in this case is to select additional registration targets manually in a few images and perform a preliminary multipoint calibration (step 3). In either case, after registration targets have been selected (mostly automatically) for a sufficiently wide range of model attitude settings, a multipoint calibration is performed (step 3) to obtain precise values for all camera parameters and all model alignment parameters. This completes the calibration process. After this (step 4) model position and attitude determination can be performed using automatic image registration. In luminescent paint measurements an additional task is to map processed image data onto a three-dimensional grid of the test article. This task can be interpreted as calculating model coordinates (x_i, y_i, z_i) for measured image coordinates (u_{kci}, v_{kci}).[7]

A possible variation to step 1 would be to determine the interior parameters of the cameras in a laboratory calibration[1,17] and keep them fixed in the single- and multipoint calibrations from Table 1. This approach is preferred if accurate laboratory calibrations are available.

E. Least-Squares Optimization

Steps 1b, 3, 4, and 5 in Table 1 involve determination of a set of parameters through iterative least-squares optimization. To do this, the theoretical model that is constituted by Eqs. (1–9) is written symbolically as

$$u_{kci} = u_{kci}(\boldsymbol{p}), \qquad v_{kci} = v_{kci}(\boldsymbol{p}) \tag{10}$$

Here, the vector $\boldsymbol{p}$ represents the set of unknown parameters. For example, in step 1b these would be the five interior and six exterior parameters for a specific camera. Let measured image coordinates be denoted with a tilde. The task of determining a parameter vector $\boldsymbol{p}$ can thus be interpreted as minimizing the least-squares sum

$$\chi^2(\boldsymbol{p}) \equiv \sum_k \sum_c \sum_i \left\{ [u_{kci}(\boldsymbol{p}) - \tilde{u}_{kci}]^2 + [v_{kci}(\boldsymbol{p}) - \tilde{v}_{kci}]^2 \right\} \tag{11}$$

The sums over the attitude settings k and the camera indices c can involve either a single or multiple elements, as indicated in the

Table 1 Photogrammetry tasks for wind-tunnel testing

Step	Task	Image coordinates u_{kci}, v_{kci}	Target model coordinates x_i, y_i, z_i	Camera interior parameters u_c, v_c, f_c, a_c, K_{1c}	Camera exterior parameters x^*_c, y^*_c, z^*_c, ϕ^*_c, κ^*_c, ω^*_c	Model alignment Δx_m, Δy_m, Δz_m, α_m, β_m, ϕ_m	Model position and attitude Δx_k, Δy_k, Δz_k, α_k, β_k, ϕ_k	Number of attitude settings Σ_k	Number of cameras Σ_c
1a	Estimate camera parameters	K[a]	K	**Calculate** (from DLT, with $K_{1c} = 0$)	**Calculate** (from DLT)	K (nominal values)	K (sting values)	One only	One at a time
1b	Single-point camera calibration	**Calculate**	K	**Iterate** (from step 1a)	**Iterate** (from step 1a)	K (nominal values)	K (sting values)	One only	One at a time
2[b]	Predict target positions	K	K	K	K	K	K (sting values)	One at a time	One at a time
3	Multipoint camera calibration	K	K	**Iterate** (from step 1b)	**Iterate** (from step 1b)	**Iterate** (from sting values)	K (sting values)	Series of wind-off images	All at once
4	Determine model P&A	K	K	K	K	K	**Iterate** (from sting values)	One at a time	All at once
5	Check camera motion	K	K	K	**Iterate** (from step 3)	K	K (from step 4)	One at a time	One at a time

[a]K = known. [b]Step 2 enables automatic image registration for subsequent application of steps 3 and 4.

right-hand columns in Table 1. The sum over i involves all targets that are seen in the image associated with camera c and attitude setting k. Closely associated with the χ^2 merit function from Eq. (11) is the rms fit error

$$\sigma(\boldsymbol{p}) \equiv [(1/N)\chi^2(\boldsymbol{p})]^{\frac{1}{2}} \tag{12}$$

where N denotes the total number of image coordinate pairs in Eq. (11). This error gives the rms deviation (in pixels) between measured and fitted image coordinates. In Ref. 1 Liu et al. approach minimization of a merit function similar to that of Eq. (11) in two steps, by separating interior and exterior camera parameters. Likewise, in Ref. 2 minimization of Eq. (11) is broken into steps, by separating camera parameters and model alignment parameters. Subsequent work by the author has indicated that it is more efficient to fit all data simultaneously, though this requires combining data from multiple model attitude settings and from multiple cameras. This is the approach advocated here. To implement it, a Levenberg Marquardt (LM) algorithm was adapted for iteratively minimizing the merit function from Eq. (11).[18] At the heart of the algorithm, a subroutine must be specified, which for a single target point i produces both the values of the image coordinates u_{kci} and v_{kci} (considered functions in the parameter vector $\boldsymbol{p}$) and the derivatives of these coordinates with respect to the fit parameters. Calculation of the derivatives is straightforward by application of the chain rule to Eqs. (1–9) and Eq. (A1). [For the distortion terms from Eqs. (5), it suffices to consider the derivative with respect to K_{1c} only.] From the derivatives the so-called curvature matrix must be calculated for use by the LM algorithm. For Eq. (11) the elements of this matrix are given by

$$\alpha_{mn} \equiv \sum_k \sum_c \sum_i \left\{ \frac{\partial u_{kci}}{\partial p_m}\frac{\partial u_{kci}}{\partial p_n} + \frac{\partial v_{kci}}{\partial p_m}\frac{\partial v_{kci}}{\partial p_n} \right\} \tag{13}$$

where m and n each vary over all components of the fit parameter vector $\boldsymbol{p}$. For each of the iterative tasks from Table 1, it is indicated how initial values of the fit parameters can be obtained. Experience has shown that satisfactory convergence of the LM algorithm is typically reached in 1–10 iterations, even when fitting all six model alignment parameters and up to 11 parameters (5 interior plus 6 exterior) per camera. This small number of iterations constitutes a significant speed up over the simplex method that was employed in Ref. 2. Iteration was typically terminated when the change in rms fit error reached 0.001 image pixels.

F. Precision Estimates

An important task that remains is estimation of the precision of parameters that are obtained through least-squares optimization. This is particularly true for the multipoint calibration procedure, which can give rise to an underdetermined system. For example, if the model is pitched but not yawed or rolled, it may be impossible to determine the lateral model alignment displacement Δy_m and the yaw alignment angle β_m. In this case it is desirable to fix β_m to a user-supplied value (for example, zero), so that model yaw angles β_k can still be determined. Fortunately, estimation of the precision of fitted parameters can easily be accomplished as a postprocessing step to the LM algorithm. Two methods are employed. The first is based on calculation of the covariance matrix. This is the inverse of the curvature matrix from Eq. (13), evaluated at the final values of the fitted parameters. Let the diagonal elements of the covariance matrix be denoted by C_{mm}. The precision of fit parameter p_m (that is, the mth component of the parameter vector $\boldsymbol{p}$) can then be estimated as the probable standard error[18]

$$\sigma_{p_m} = [N/(2N - M)]^{\frac{1}{2}}\sigma(\boldsymbol{p})C_{mm}^{\frac{1}{2}} \tag{14}$$

Here, $\sigma(\boldsymbol{p})$ is the rms fit error from Eq. (12), N is the number of image coordinate pairs in the fit, and M is the number of fit parameters. The factor $2N - M$ thus represents the number of degrees of freedom of the fit. When the estimated precision is large (for example, an order of magnitude larger than the absolute value of the fitted parameter), it is advisable to fix this parameter at a user-selected value and repeat the fit.

Strictly speaking, use of Eq. (14) assumes that measurement errors are normally distributed. In practice, it is usually not known whether this is the case. To assess the possible effects of nonnormal measurement errors, a second method is used in Sec. III to estimate the precision of fitted parameters. This is the so-called bootstrap method,[18] in which a set of to-be-fitted data is replaced with a set of equal size, in which each point is a point from the original set, but drawn randomly with replacement (that is, in a typical drawing some points are omitted while others are duplicated). The new set of data is then fit in the usual way. When this procedure is repeated, e.g., 100 times, the precision of the fitted parameters from the original data set can be estimated as the square root of the variance of the fitted parameters from the randomized sets. Examples of both types of precision estimates are given in Sec. III.

III. Application Examples

To illustrate the theory from Sec. II, some results are reported that were obtained on pressure-sensitive paint tests of an evolved expendable launch vehicle (EELV; see Fig. 3b)[15] and an F-16C (Fig. 3a).[19] Both tests were performed in AEDC's 16-ft transonic wind tunnel, with eight charge-coupled device (CCD) cameras mounted as shown in Fig. 1. Both test articles were nominally 6 ft long. (Only the lower part of the EELV was viewed.) Cameras were reoriented, refocused, and rezoomed (28–41 mm) between the two tests. Images sizes were $1024 \times 1024 \times 16$ bit. Subpixel centering of imaged targets was achieved using 16-bit centroiding, with an estimated accuracy of 0.1 image pixels. (A more accurate technique has since been developed based on template matching.[20]) Average numbers of registration targets per image were 44 for the EELV and 34 for the F-16C. Targets are distributed roughly uniformly across the surface (see Fig. 6 in Ref. 15 for the EELV and Fig. 7 in Ref. 20 for the F-16C), with sufficient three-dimensional variation to use the direct linear transform to obtain initial values for the LM fitting scheme.

Table 2 summarizes results of the multipoint camera and model alignment calibrations for both tests. Principal point locations were fixed at the centers of the CCD arrays (that is, $u_c = v_c = 512$), and row-column spacing ratios were set equal to unity (that is, $a_c = 1$). Attempts to fit these parameters based on the wind-tunnel data were found to produce values that deviate more from the selected nominal values than was deemed likely (with u_c and v_c in the range 473–543 and a_c in the range 0.996–1.004), presumably as a result of projective coupling of the fitted parameters. Prerun and postrun wind-off images were combined in the calibrations, giving a total of 80×8 images for the EELV (pitch and roll) and 34×8 images for the F-16C (pitch only). Combining prerun and postrun data in this way has the advantage that small changes in camera orientation as a result of thermal effects in the tunnel[2] are mitigated at the expense of slightly higher rms fit errors [for example, $\sigma(\boldsymbol{p}) = 0.57$ pixels for prerun and postrun F-16C data combined (see table footer), vs $\sigma(\boldsymbol{p}) = 0.42$ pixels rms for prerun and postrun data separately]. Figure 4 shows that between tests, as well as between cameras, a consistent dependence of radial distortion on principal distance is found. Covariance-based precision estimates of fitted parameters from Eq. (14) are listed under "SigCov" in Table 2. Precision estimates based on the bootstrap method (with random draws performed on images as a whole) are listed under "BSFac" and are given as

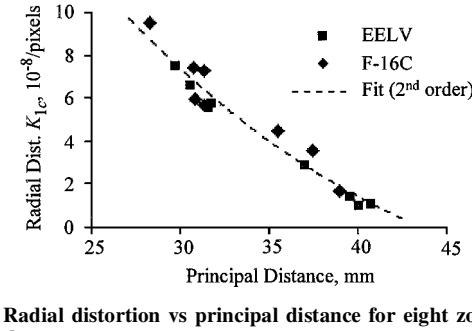

Fig. 4 Radial distortion vs principal distance for eight zoom lenses employed.

Table 2 Wind-off calibration summary

	EELV			F-16C		
Parameter	Range/value	SigCov[a]	BSFac[b]	Range/value	SigCov[c]	BSFac[b]
u_c, pix	512	Fixed	——	512	Fixed	——
v_c, pix	512	Fixed	——	512	Fixed	——
f_c, pix (24 μm/pix)	1230–1670	1.2	1.3	1189–1598	3.4	1.1
a_c	1	Fixed	——	1	Fixed	——
K_{1c}, 1E-8/pix^2	1.0–7.5	0.06	0.9	2.3–10.5	0.12	1.0
Cam. position, in.	Various	0.081	1.7	Various	0.17	1.2
Cam. angles, deg	Various	0.026	2.9	Various	0.039	1.7
Δx_m, in.	−55.716	0.0056	4.0	61.804	0.0039	2.0
Δy_m, in.	0.0701	0.0015	1.9	0	Fixed	——
Δz_m, in.	0.0131	0.0016	2.0	9.964	0.0030	4.1
α_m, deg	−0.155	0.009	5.7	0	Fixed	——
β_m, deg	90.012	0.0009	2.8	179.843	0.025	1.6
ϕ_m, deg	−90.010	0.0010	2.8	180.396	0.0087	4.2

[a]Based on $\sigma(\boldsymbol{p}) = 0.62$ pix.
[b]Factor by which bootstrap rms error exceeds covariance rms error SigCov.
[c]Based on $\sigma(\boldsymbol{p}) = 0.57$ pix.

Table 3 Wind-on position and attitude determination

	EELV (Mach = 0.7–1.2)			F-16C (Mach = 1.0)		
Parameter	Range	SigCov[a]	BSFac[b]	Range	SigCov[c]	BSFac[b]
Δx_k, in.	−0.15 to −0.03	0.0023	5.4	−0.48 to 0.02	0.0035	5.5
Δy_k, in.	−0.06 to 0.02	0.0069	2.1	−0.02 to 0	0.0062	2.7
Δz_k, in.	−0.09 to 0.04	0.0068	2.3	−1.3 to 0.0	0.0070	2.2
α_k, deg	−6 to 6	0.010	1.4	0 to 26	0.015	1.2
β_k, deg	−0.05 to 0.16	0.010	1.5	0.00 to 0.03	0.013	1.3
ϕ_k, deg	−47 to 154	0.019	3.3	0 to 0.16	0.033	1.7

[a]Based on $\sigma(\boldsymbol{p}) = 0.77$ pix.
[b]Factor by which bootstrap rms error exceeds covariance rms error SigCov.
[c]Based on $\sigma(\boldsymbol{p}) = 0.84$ pix.

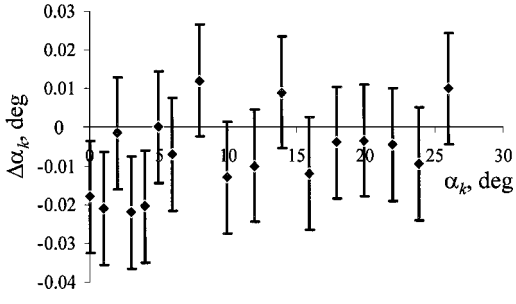

Fig. 5 Example of wind-off deviation of photometrically determined pitch angle from tunnel inclinometer angle for F-16C.

a multiple of the covariance-based values. For example, the bootstrap precision for the model alignment factor Δx_m for the EELV is 4.0×0.0056 in. BSFac values range from 0.9 to 5.7. On average, bootstrapping thus gives a more conservative estimate of the precision of the fitted parameters than does the covariance-matrix formalism.

Table 3 summarizes results of six-parameter position and attitude (P&A) determinations at wind-on conditions for the same tests, with 99×8 images for the EELV and 17×8 images for the F-16C. Least-squares fits were performed on sets of eight images at a time, with one image from each camera. Again, bootstrapping (with random draws performed on the eight available images per test point) produces more conservative precision estimates than does the covariance-matrix formalism, though less so for attitude than for position. The precision of the photogrammetrically derived attitude angles is on the order of 0.010–0.015 deg for pitch and yaw and about 0.04 deg for roll. These precision values reflect, in part, motion of the cameras during the test as a result of thermal effects in the tunnel, as well as deformation of the test article (in particular, the F-16C at high angles of attack). For example, when performing the same six-parameter P&A fits on wind-off data rms fit errors and P&A precision estimates are roughly half of those at wind-on conditions. To assess the absolute accuracy of the results, a comparison was made between photogrammetrically determined pitch angles and inclinometer-based values (with an estimated accuracy of 0.002 deg) for the F-16C test. Figure 5 shows that the difference (0.010 deg rms) between these two sets of values is consistent with the calculated precision (0.015 deg rms) of the photogrammetrically determined values.

IV. Conclusions

A comprehensive mathematical model has been demonstrated for the application of photogrammetry in wind-tunnel testing. The model emphasizes not only the usual calibration of the interior parameters of the cameras, but also the placement of multiple cameras as well as the test article itself relative to the tunnel. Model position and attitude measurements are thus aligned with the pitch and roll axes of the tunnel. This is accomplished by combining data from multiple cameras and multiple attitudes of the model support system in a least-squares fit, with up to 94 fitted parameters (6 for model attitude and 11 per camera for eight cameras). Fitted parameters are suitably averaged over the available data points in this way, and precision estimates for the fitted parameters can be computed either by use of the covariance-matrix formalism or by bootstrapping. The mathematical model also plays the important role of producing estimates for image coordinates of registration targets based on readout values of the model support system, thus allowing automatic image registration according to Ref. 14.

Once calibrated, data from multiple cameras can be combined to determine the position and attitude of the test article during a wind-tunnel test. At the present time the absolute accuracy for pitch measurements appears to be on the order of 0.01 deg. It is estimated that this value can be lowered by an order of magnitude if three improvements are implemented: 1) zoom lenses are replaced by fixed focal length lenses; 2) interior parameters of the cameras are determined through independent laboratory calibration (leaving

only the camera exterior parameters to be determined relative to the wind tunnel); and 3) cameras are mounted such that motion caused by thermal expansion of the tunnel is minimized. These improvements are not critical for the type of data for which the mathematical model has been demonstrated (that is, pressure-sensitive paint measurements), but would be desirable for an optical system that is dedicated to attitude measurements.

Appendix A: Euler Orientation Matrix

The following three-angle Euler orientation matrix is used for model alignment, model attitude, and camera orientation (other choices are possible):

$$\boldsymbol{R}(\alpha, \beta, \phi) = \begin{pmatrix} c_\alpha c_\beta & s_\beta c_\phi + s_\alpha c_\beta s_\phi & -s_\beta s_\phi + s_\alpha c_\beta c_\phi \\ -c_\alpha s_\beta & c_\beta c_\phi - s_\alpha s_\beta s_\phi & -c_\beta s_\phi - s_\alpha s_\beta c_\phi \\ -s_\alpha & c_\alpha s_\phi & c_\alpha c_\phi \end{pmatrix} \tag{A1}$$

where $s_\alpha = \sin\alpha$, $c_\alpha = \cos\alpha$, $s_\beta = \sin\beta$, $c_\beta = \cos\beta$, $s_\phi = \sin\phi$, and $c_\phi = \cos\phi$. This is the standard form for AEDC's 16-ft transonic wind tunnel, with tunnel coordinate axes as shown in Fig. 3 and angles applied in the order yaw β, pitch α, roll ϕ. The following sign conventions apply: nose to left (that is, up out of paper in Fig. 3) for positive β, nose up for positive α, and left wing up for positive ϕ. In Eq. (3) the matrix from Eq. (A1) is applied also to specify the orientations of the cameras. This is consistent with standard photogrammetry notation,[1,12,13] except for a sign change on the angles ϕ_c^* and ω_c^* in Eq. (3).

Appendix B: Direct Linear Transform

In the direct linear transform (DLT) formulation the image coordinates of a point i on the test article with model coordinates (x_i, y_i, z_i) are expressed as[1,7,16]

$$u_{kci} = \frac{L_1 x_i + L_2 y_i + L_3 z_i + L_4}{L_9 x_i + L_{10} y_i + L_{11} z_i + 1}$$

$$v_{kci} = \frac{L_5 x_i + L_6 y_i + L_7 z_i + L_8}{L_9 x_i + L_{10} y_i + L_{11} z_i + 1} \tag{B1}$$

The dependence of the DLT coefficients $L_1 \ldots L_{11}$ on the model attitude setting k and the camera index c is not indicated explicitly. By multiplying out the denominators in Eq. (B1), linear expressions in the DLT coefficients are obtained. The coefficients $L_1 \ldots L_{11}$ can then be obtained from a set of measured image coordinates by a noniterative (that is, direct) solution of the least-squares normal equations. From these, starting values for the iterative single-point calibration from step 1b in Table 1 can be obtained. First, the DLT coefficients are converted to projective transform coefficients. Second, the resulting exterior camera parameters are transformed from model coordinates to tunnel coordinates.

To convert the DLT coefficients to projective transform coefficients, radial distortion is neglected, that is, $K_{1c} = 0$. Also, Eq. (2) is expressed in model coordinates according to

$$U_{kci} = u_{xkc}(x_i - x_{kc}) + u_{ykc}(y_i - y_{kc}) + u_{zkc}(z_i - z_{kc}) \tag{B2}$$

Similar expressions apply for V_{kci} and W_{kci}. The results from Eqs. (1) and (B2) can be recast in the form of Eq. (B1). This yields expressions for $L_1 \ldots L_{11}$ in terms of the projective transform parameters u_c, v_c, f_c, a_c, x_{kc}, y_{kc}, z_{kc}, u_{xkc}, u_{ykc}, u_{zkc}, v_{xkc}, v_{ykc}, v_{zkc}, w_{xkc}, w_{ykc}, and w_{zkc}. These expressions can be inverted to obtain the projective transform parameters in terms of $L_1 \ldots L_{11}$ [for example, see Ref. 12, but with a minus sign added to Eq. (4.44)]. Let the implied camera position be denoted by $\boldsymbol{x}_{kc}$. This vector transforms from model coordinates to tunnel coordinates in the same way as the vector $\boldsymbol{x}_i$ in Eqs. (6) and (8′). It thus follows that the exterior camera position relative to the tunnel can be calculated according to

$$\boldsymbol{x}_c^* = \Delta\boldsymbol{x}_{0k} + \boldsymbol{R}_{0k}[\Delta\boldsymbol{x}_m + \boldsymbol{R}_m\boldsymbol{x}_{kc}] \tag{B3}$$

Likewise, let the camera orientation matrix relative to the model coordinate system be denoted by $\boldsymbol{m}_{kc}$, analogous to Eq. (3). This matrix transforms according to

$$\left[\boldsymbol{m}_c^*\right]^T = \boldsymbol{R}_{0k}\boldsymbol{R}_m\boldsymbol{m}_{kc}^T \tag{B4}$$

The origin of the transposes in Eq. (B4) is that the rows (that is, not the columns) of the matrices $\boldsymbol{m}_{kc}$ and $\boldsymbol{m}_c^*$ correspond to vectors in three-dimensional space [see Eq. (3) and Fig. 2]. Given the matrix $\boldsymbol{m}_c^*$, values for the camera tunnel angles ϕ_c^*, κ_c^*, and ω_c^* can be extracted using Eqs. (3) and (A1). In so doing, it does not matter which of the two possible solutions is chosen.

Acknowledgments

Discussions with my colleagues D. W. Sinclair, M. E. Sellers, D. M. Cahill, and F. W. Steinle Jr. are appreciated, as are suggestions by the anonymous referees. The research reported herein was performed by the Arnold Engineering Development Center (AEDC), Air Force Materiel Command. Work and analysis for this research were performed by personnel of Jacobs Sverdrup, AEDC Group, technical services contractor for AEDC. Further reproduction is authorized to satisfy needs of the U.S. Government.

References

[1]Liu, T., Cattafesta, L. N., III, Radeztsky, R. H., and Burner, A. W., "Photogrammetry Applied to Wind-Tunnel Testing," *AIAA Journal*, Vol. 38, No. 6, 2000, pp. 964–971.

[2]Ruyten, W., "Toward an Integrated Optical Data System for Wind-Tunnel Testing," AIAA Paper 99-0181, Jan. 1999; also Ruyten, W., "Model Attitude Determination in Wind Tunnel with a Luminescent Point Data System," *AIAA Journal*, Vol. 38, No. 9, 2000, pp. 1692–1697.

[3]Burner, A. W., Fleming, G. A., and Hoppe, J. C., "Comparison of Three Optical Methods for Measuring Model Deformation," AIAA Paper 2000-0835, Jan. 2000.

[4]Burner, A. W., and Martinson, S. D., "Automated Wing Twist and Bending Measurements Under Aerodynamic Load," AIAA Paper 96-2253, June 1996.

[5]Bell, J. H., and Burner, A. W., "Data Fusion in Wind Tunnel Testing; Combined Paint and Model Deformation Measurements," AIAA Paper 98-2500, June 1998.

[6]Liu, T., Radeztsky, R., Garg, S., and Cattafesta, L., "A Videogrammetric Model Deformation System and Its Integration with Pressure Paint," AIAA Paper 99-0568, Jan. 1999.

[7]Bell, J. H., and McLachlan, B. G., "Image Registration for Luminescent Paint Sensors," AIAA Paper 93-0178, Jan. 1993; also Bell, J. H., and McLachlan, B. G., "Image Registration for Pressure-Sensitive Paint Applications," *Experiments in Fluids*, Vol. 22, No. 1, 1996, pp. 78–86.

[8]Chen, F.-J., "Application of Least-Squares Adjustment Technique to Geometric Camera Calibration and Photogrammetric Flow Visualization," *43rd International Instrumentation Symposium*, Instrumentation Society of America, Research Triangle Park, NC, 1997, pp. 659–668.

[9]Cattafesta, L. N., III, and Moore, J. G., "Review and Application of Non-Topographic Photogrammetry to Quantitative Flow Visualization," AIAA Paper 96-2180, June 1996.

[10]Fuykschot, P. H., "Vibration Compensation of Gravity Sensing Inclinometers in Windtunnel Testing," *42nd International Instrumentation Symposium*, Instrumentation Society of America, Research Triangle Park, NC, 1996, pp. 493–503.

[11]Burner, A. W., and Liu, T., "Videogrammetric Model Deformation Measurement Technique," *Journal of Aircraft*, Vol. 38, No. 4, 2001, pp. 745–754.

[12]McGlone, J. C., "Analytic Data Reduction Schemes in Non-Topographic Photogrammetry," *Non-Topographic Photogrammetry*, 2nd ed., edited by H. M. Karara, American Society of Photogrammetry and Remote Sensing, Falls Church, VA, 1989, Chap. 4.

[13]Wong, K. W., "Basic Mathematics of Photogrammetry," *Manual of Photogrammetry*, 2nd ed., edited by C. C. Slama, American Society of Photogrammetry, Falls Church, VA, 1980, Chap. 2.

[14]Ruyten, W., "Automatic Registration of Luminescent Paint Images," *45th International Instrumentation Symposium*, Instrumentation Society of America, Research Triangle Park, NC, 1999, pp. 279–288.

[15]Ruyten, W., "Model Attitude Measurements with an Eight-Camera Pressure-Sensitive Paint System," AIAA Paper 2000-0831, Jan. 2000.

[16]Abdel-Aziz, Y. I., and Karara, H. M., "Direct Linear Transformation from Comparator Coordinates into Object Space Coordinates in Close-Range Photogrammetry," *Proceedings of the ASP/UI Symposium on Close-Range Photogrammetry*, Univ. of Illinois, Urbana, IL, 1971, pp. 1–18.

[17]Burner, A. W., "Zoom Lens Calibration for Wind Tunnel Measurements," *Videometrics IV*, Vol. 2598, Society of Photo-Optical Instrumentation Engineers, Philadelphia, 1995, pp. 19–33.

[18]Press, W. H., Teukolsky, S. A., Vetterling, W. T., and Flannery, B. P., *Numerical Recipes in Fortran*, 2nd ed., Cambridge Univ. Press, New York, 1992, Chap. 15.

[19]Sellers, M. E., "Application of Pressure Sensitive Paint for Determining Aerodynamic Loads on a Scale Model of the F-16C," AIAA Paper 2000-2528, June 2000.

[20]Ruyten, W. M., "Subpixel Localization of Synthetic References in Digital Images by Use of Noncomposite and Composite Augmented Templates," *Image Processing: Algorithms and Systems*, edited by E. R. Dougherty, J. T. Astola, and K. O. Egiazarian, *Proceedings of the Society of Photo-Optical Instrumentation Engineers*, Vol. 4667 (to be published).

R. P. Lucht
Associate Editor